Journal of Rock Mechanics and Geotechnical Engineering 14 (2022) 663–669

Contents lists available at ScienceDirect

Journal of Rock Mechanics and Geotechnical Engineering

journal homepage: www.jrmge.cn

Technical Note

A fiber Bragg grating based earth and water pressures transducer with three-dimensional fused deposition modeling for soil mass

Yue Qin, Qiankun Wang, Dongsheng Xu*, Jiaming Yan, Shanshan Zhang

School of Civil Engineering and Architecture, Wuhan University of Technology, Wuhan, 430070, China

ARTICLE INFO

Article history:
Received 22 March 2021
Received in revised form
3 June 2021
Accepted 17 July 2021
Available online 20 September 2021

Keywords:
Fused deposition modeling (FDM)
Fiber bragg-grating (FBG) sensor
Earth pressure
Water pressure

ABSTRACT

A novel fiber Bragg grating (FBG) sensor with three-dimensional (3D) fused deposition modeling (FDM) approach is proposed for effective stress measurement in soil mass. The three-diaphragm structure design is developed to measure earth and water pressures simultaneously. The proposed transducer has advantages of small size, high sensitivity, low cost, immunity to electromagnetic interference and rapid prototyping. The working principle, design parameters, and manufacturing details are discussed. The proposed transducer was calibrated for earth and water pressures measurement by using weights and a specially designed pressure chamber, respectively. The calibration results showed that the wavelength of the transducer was proportional to the applied pressure. The sensitivity coefficients of the earth and water pressures were 12.633 nm/MPa and 6.282 nm/MPa, respectively. Repeated tests and error analysis demonstrated the excellent stability and accuracy of the earth and water pressure measurements. The performance of the proposed transducer was further verified by a model experimental test and numerical analysis, which indicated that the proposed transducer has great potential for practical applications.

1. Introduction

Earth pressure measurement is of great significance to ensure safe design in geotechnical engineering (Zhu et al., 2012, 2015). The earth pressure normally consists of soil stress induced among soil particles and pore water pressure in the soil mass. The stress transferred between soil particles is the effective stress, which cannot be measured directly. Commonly used earth pressure transducers measure the total earth pressure, which cannot be decoupled from the pore water pressure. In general, there are five types of sensing technologies used for earth pressure measurement, such as the electromagnetic transducer, inductive pressure transducer, capacitive pressure transducer, vibration wire strain gauge transducer and fiber optic sensor (Pachava et al., 2014; Xu et al., 2017, 2018; Zhou et al., 2018). These strain gauges or fiber optic sensors are typically glued onto a membrane that is in contact with soil mass.

The application of traditional transducers is limited by their susceptibility to anti-electromagnetic interference and poor long-term reliability in harsh environments (Zhu et al., 2014; Xu et al., 2019; Wang et al., 2020). Fiber optic transducers are ubiquitous in engineering applications because of their resistance to anti-electromagnetic interference, high accuracy, long-term stability, and parallel connectivity (Singh et al., 2017; Xu, 2017; Zhou et al., 2019). Many researchers have demonstrated the effectiveness and efficiency of fiber optic sensors in various engineering practices (Zhu et al., 2017; Xu et al., 2020a, b; Wu et al., 2020; Li et al., 2021).

With the development of three-dimensional (3D) printing, the fused deposition modeling (FDM) approach has been introduced into the integrated manufacturing and packaging of transducers (Tang et al., 2018; Wei et al., 2018; Meng et al., 2020; Pei et al., 2020; Song et al., 2020). Gu et al. (2016) proposed a fiber optic transducer for measuring hydraulic pressure by observing the deformation of the fiber grating attached to the outer wall of a thin-walled cylinder. Hong et al. (2016) designed a fiber grating pressure transducer, manufactured by 3D printing, to measure the vertical pressure. Zhang et al. (2017) designed a shock-resistant fiber grating pressure transducer, accompanied by a flat diaphragm as the force-loading

* Corresponding author.
E-mail address: dsxu@whut.edu.cn (D. Xu).
Peer review under responsibility of Institute of Rock and Soil Mechanics, Chinese Academy of Sciences.

https://doi.org/10.1016/j.jrmge.2021.07.009

surface, which was successfully applied in explosion experiments. Hu et al. (2018) presented a fiber grating inclinometer transducer for highway slope monitoring and early warning systems, which could assist engineers to adopt quick and essential measures to deal with potential landslide risks. Hong et al. (2019a, b, c) studied the effectiveness and efficiency of FDM as the manufacturing and packaging method of fiber optic transducers. Yang et al. (2019) adopted the fiber grating and 3D printing to design a new type of hoop strain transducer, finding good results in calibration and uniaxial compression tests.

Determination of effective earth pressure is challenging as the earth pressure transducer itself would affect the pore water pressure distribution at the same point in soil mass (Zhou and Qi, 2019; Xu et al., 2020c; Cui et al., 2021). The effective earth pressure was calculated from the measured results of total earth pressure and pore water pressure which were measured by two independent transducers. This approach would result in large measurement errors (Li et al., 2017; Zhao et al., 2018). Thus, this study proposed an earth/water pressure hybrid transducer fabricated by the FDM technology which can obtain the effective stress directly under fully saturated conditions. The working principle and design details of the transducer are introduced. The results of calibration and model validation tests are carried out and discussed.

2. The hybrid FBG-based earth/water pressure transducer

2.1. Working principle

The fiber Bragg grating (FBG) sensor was fabricated by a phase mask method in this study. The length of Bragg grating was 10 mm. The working principle of the FBG is shown in Fig. 1. As the broadband laser source injected into the optical fiber, a narrow band wavelength will be reflected and recorded by the optical interrogator. As described by the coupled-mode theory, narrowband light of a certain wavelength is reflected because of the periodic structure of refractive indices when a beam of broadband light is incident on the grating. The wavelength of the reflected light is sensitive to the environmental strain and temperature. Thus, the reflected wavelength of the FBG sensor have a linear relationship with the strain and temperature, which can be expressed as follows (Hill and Meltz, 1997; Majumder et al., 2008; Garcia-Miquel, 2016):

$$\frac{\Delta\lambda}{\lambda} = c_1\varepsilon + c_2\Delta T \tag{1}$$

where λ is the reference wavelength at the initial conditions; $\Delta\lambda$ is the wavelength drift due to the external strain ε and temperature variation ΔT; and c_1 and c_2 are the strain and temperature coefficients, respectively. The coefficients c_1 and c_2 are constants with values of $c_1 = 0.78 \times 10^{-6}$ and $c_2 = 6.67 \times 10^{-6}\ ^\circ\mathrm{C}^{-1}$. Thus, the strain can be obtained by Eq. (1) according to the measurement of wavelength drift $\Delta\lambda$ with the compensated temperature effect.

2.2. Design and fabrication process

A detailed view and the three-layer structure of the proposed hybrid transducer is displayed in Fig. 2b. The upper circular diaphragm I, used to measure the overburden earth pressure, was set with a groove on its lower side. The groove was 0.5 mm in depth, which was the minimum resolution of the 3D printer. The FBG sensor was installed in the groove with the tension state. The A_I side would bear the overburden earth pressure during testing and

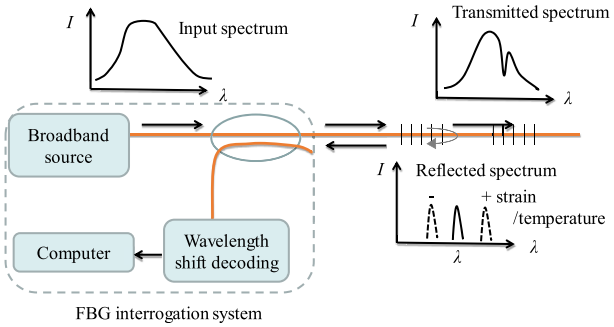

Fig. 1. Sensing principle of fiber Bragg-grating sensor.

thus the tensile deformation occurred on the B_I side. The deformation of the membrane would result in the wavelength shift of the FBG sensors. The middle layer circular diaphragm II was used to measure the water pressure. The groove with the depth of 0.5 mm was fabricated on the tension side to install FBG sensors. When the water pressure was applied to the A_{II} side of the diaphragm II, the FBG in the groove on the B_{II} side would be stretched and the following shifted wavelength could be further used to calculate the strain (i.e. ε_{BII}). An additional FBG sensor was installed on the A_{II} side to measure bending strain (ε_{AII}). Thus, the bending strain induced by the water pressure could be obtained by $(\varepsilon_{BII} - \varepsilon_{AII})/2$ and the temperature strain could be calculated by $(\varepsilon_{BII} + \varepsilon_{AII})/2$. The temperature compensation should also be taken into consideration during these calculations. Normally, in experimental test conditions the temperature has low variation, therefore the temperature effect could be compensated according to the room temperature.

A certain number of micro-pores were fabricated in the diaphragm III, through which only water was allowed to flow. As shown in Fig. 2b, cavities were formed between diaphragms I and II, as well as between diaphragms II and III. The FBGs of diaphragms I and II were designed to measure the overburden earth and water pressures, respectively. The optic fibers should be carefully protected throughout the process of fabrication and application. The printing processes for diaphragms I and II was similar which were printed to a certain thickness with a groove formed according to the design scheme. During the printing, the fibers were placed into the grooves. After printing, diaphragms I, II, and III were assembled to form the hybrid FBG based earth/water pressure transducer. The data can be recorded by the FBG interrogator through the optical fibers.

Fig. 3a is the schematic diagram of the manufacturing process for the proposed transducer. The 3D FDM printing adopts specialized equipment to spray or fuse materials layer by layer to complete the production, which greatly reduces the manufacturing complexity. Printing materials were sent to the printer nozzle by the wire feeding mechanism through the processes of heating, melting and squeezing out materials to solidify layer by layer until the model was formed. The raw material was the commonly used polylactic acid (PLA), which was renewable and biodegradable with good physical properties. Fig. 3b shows the 3D printing process of the proposed hybrid transducer.

Fig. 4a shows the wavelength drift of the transducer during the printing process. The wavelength drift can be divided into three stages: before, during, and after printing. The initial wavelength of the FBG sensor was 1526.4 nm. During printing, the hot PLA material that was squeezed out from the nozzle of the 3D printer caused significant thermal expansion of the FBG sensor, which resulted in the wavelength drift with high fluctuations. When the

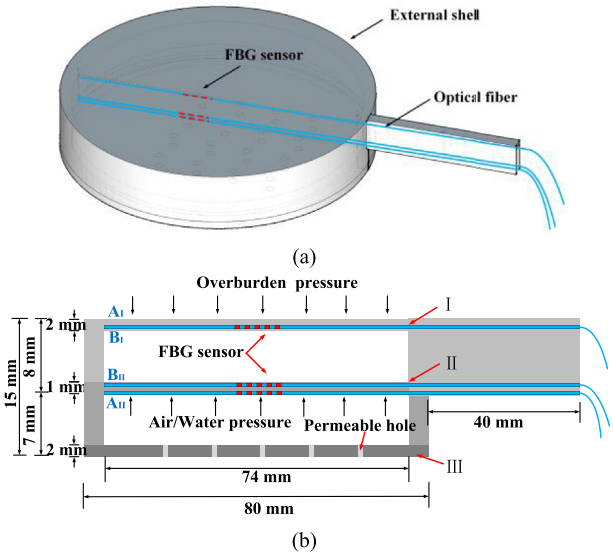

Fig. 2. Transducer design: (a) Overall geometry and (b) Main section view.

printing was completed, the wavelength drift gradually decreased with the decreasing of temperatures. The changes in wavelength throughout the process can be attributed to the expansion and shrinkage of the PLA material with its temperature fluctuations. The designed FBG transducer successfully went through the melt temperature of PLA at 210 °C without any influence. Fig. 4b shows the final printed transducer that was used for further calibration and verification.

3. Calibration test

3.1. Calibration for earth pressure

The fabricated transducer was calibrated for earth and water pressure measurements. Two FBG sensors were installed in the transducer, with an additional sensor to eliminate the temperature effect by Eq. (1). The earth pressure of the transducer was calibrated with stage loads. Three calibration tests were conducted with stages loads from 0 N to 50 N at a speed of 10 N per step. Fig. 5 shows the FBG wavelength versus the applied pressures. The wavelength was increased with the increasing of applied loads. The wavelength drift versus applied pressure is shown in Fig. 6. The results indicated that the FBG wavelength had a linear relationship with the applied pressures. The sensitivity coefficient of the corresponding pressure was 12.633 nm/MPa in the measurement range of 0–100 kPa.

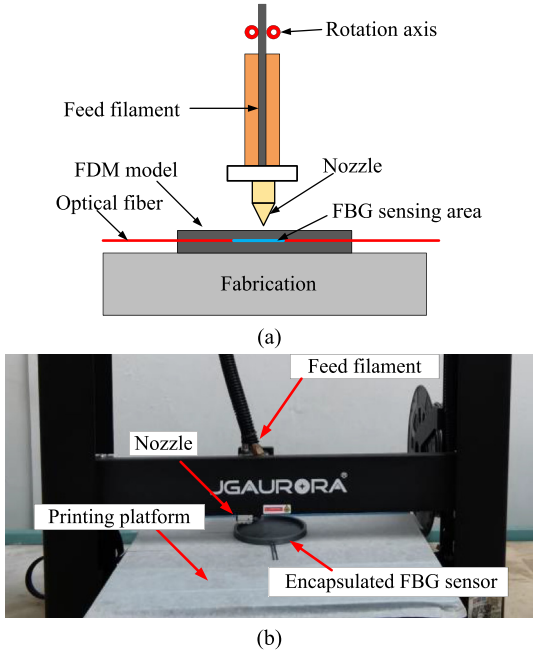

Fig. 3. Fabrication process of the FBG transducer: (a) Diagram of the 3D FDM fabrication, and (b) Photo taken during fabrication process.

3.2. Calibration for water pressure

The water/air pressure measurement by the proposed transducer was calibrated by a specialized designed system as shown in Fig. 7. In this study, the measured water pressure was calibrated by applying air pressure from an air compressor. The transducer was placed in an airtight pressure chamber, ensuring that the pressure on the transducer was stable. The signal transmission pigtail of the transducer was fed out from the pressure chamber and connected to the FBG demodulator for signal collection. There were seven cycles of loading and unloading in the calibration tests, with an applied air pressure range of 0–0.3 MPa. After pressurizing, time was required for data stabilization before continuing pressurization. A stable wavelength measurement was acquired for each air pressure level before the next air pressure level was applied.

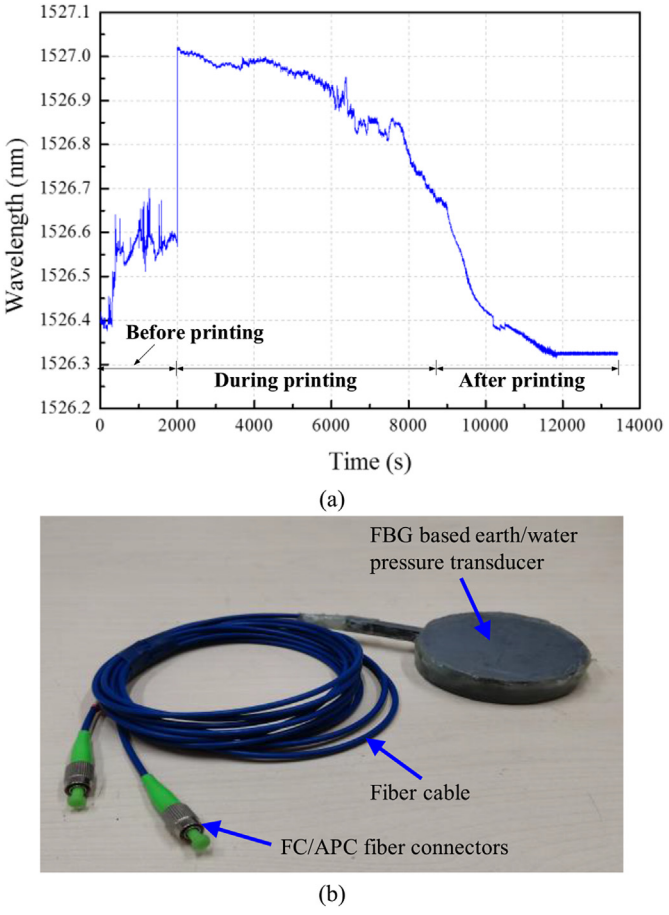

Fig. 4. Fabrication process and manufactured transducer: (a) Wavelength versus time during the 3D printing process, and (b) The printed FBG pressure transducer.

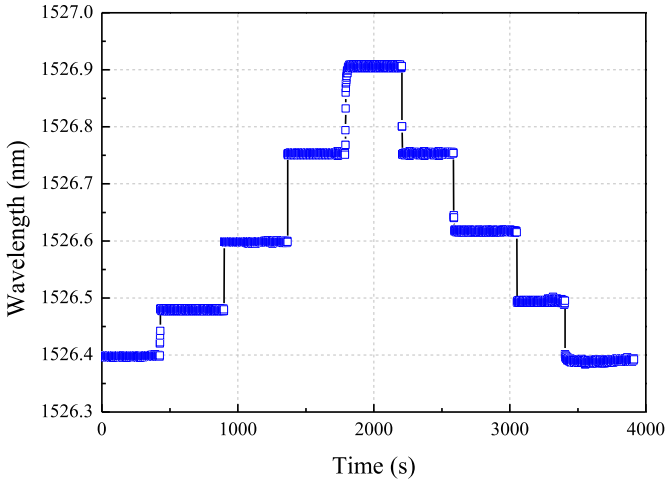

Fig. 5. Calibration results of the hybrid transducer under normal pressure.

The stability was verified by repeated experiments. Fig. 8a shows the periodic changes of wavelength during loading cycles. The wavelength was varied in an almost constant fluctuation range of 1538 nm–1541 nm when the air pressure was applied. The wavelength under each load and the average wavelength were calculated. The results indicated that the maximum error was 3.1% with a maximum absolute relative error less than 2%. The results proven that the sensor had relatively low error rates and high sensitivity. The relationship between wavelength and pressure was analyzed. As shown in Fig. 8b, the FBG pressure transducer shows good linear characteristics with a sensitivity coefficient of 6.282 nm/MPa.

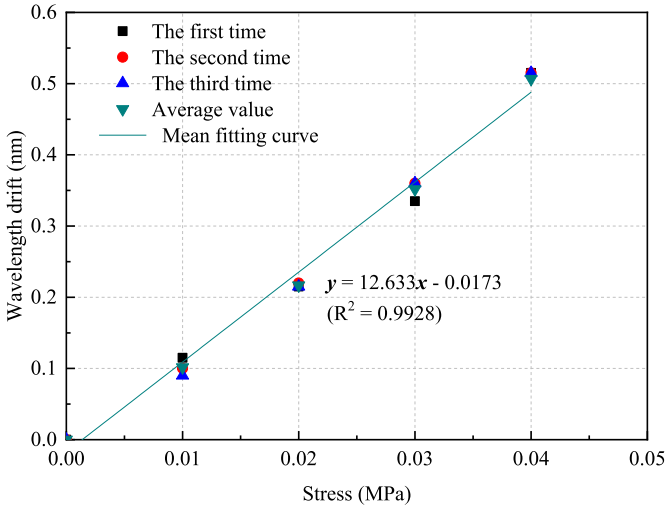

Fig. 6. Relationship between wavelength drift and stress.

4. Model test verification

4.1. Experiments for validation

The pullout experiments of anchor rod were carried out after calibration of the transducer. Fig. 9 shows the experimental setup. The transducer was placed in a physical model box which has a dimension of 60 cm in length, 22.5 cm in width and 30 cm in height. For comparisons, strain gauges were installed on the surface of the glass-fiber-reinforced polymer (GFRP) bar. The dynamic strain collector was adopted to check whether the transducer was in a normal condition. The GFRP anchor was connected to a high-strength steel wire, which was loaded step by step through weights. The wavelength were measured and recorded by the FBG demodulator. The strain gauge was connected to the dynamic strain acquisition.

Staged loads were applied by using a hydraulic jack. The earth pressures were controlled as 0.3 kN, 0.6 kN, and 0.9 kN with water pressures of 0.01 MPa, 0.02 MPa, and 0.03 MPa, respectively. Fig. 10a shows that the shifted wavelength during the experiment drifted uniformly with the applied pressure and the two wavelengths corresponding to earth and water pressures changed almost simultaneously. Fig. 10b is the pressure calculated from the wavelength of the transducer in Fig. 10a according to the previous calibration test and the change of wavelength. The earth pressure changed around 55 kPa and the water pressure changed around 7 kPa at each loading stage, demonstrating that the pressure change of the transducer was stable.

4.2. Verification with numerical analysis

Numerical analysis was carried out to further verify the accuracy of the experiment. COMSOL Multiphysics 5.6 with the structure mechanics module and Darcy's law were implemented to establish the numerical model. Fig. 11 shows the boundary conditions of the

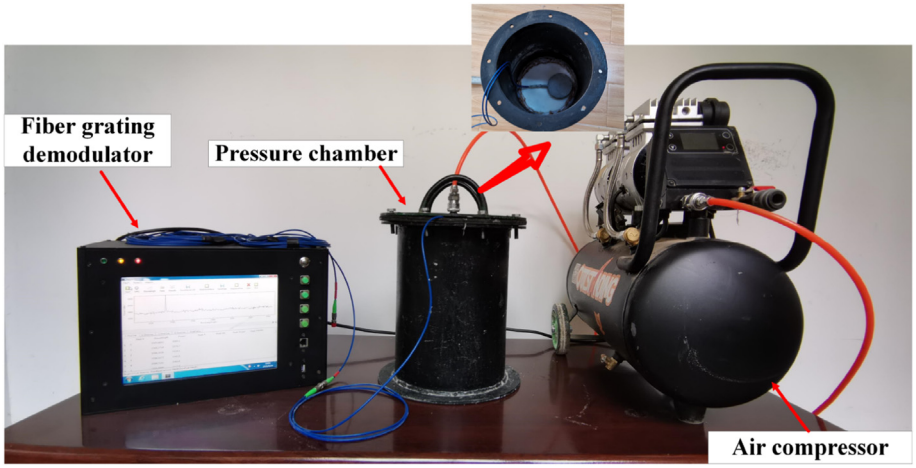

Fig. 7. Calibration system for water pressure.

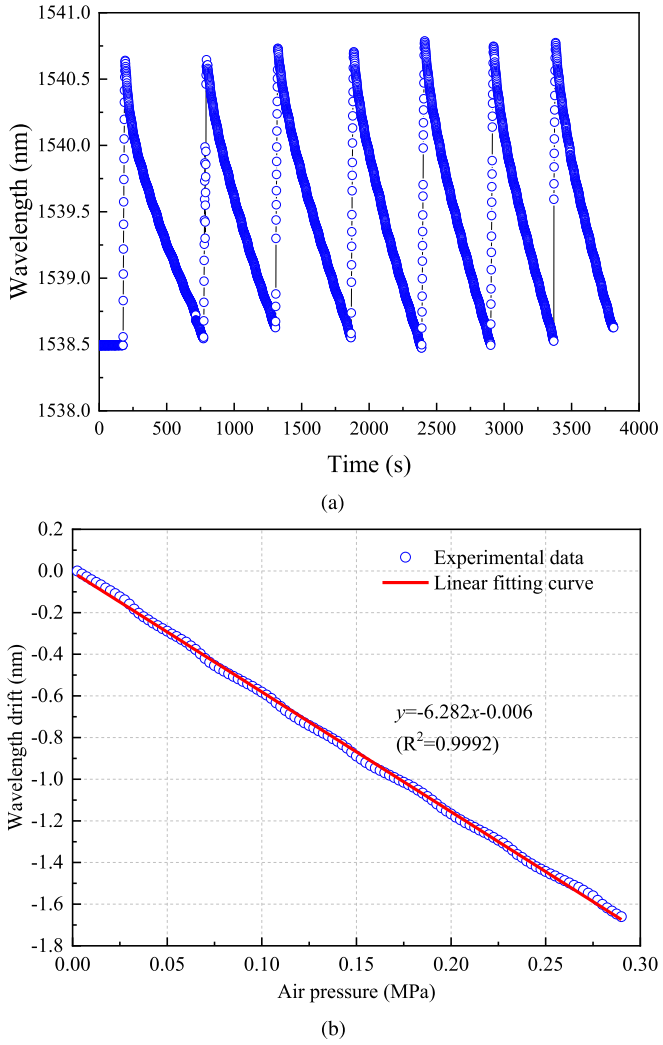

Fig. 8. Calibration results under various air pressures: (a) Wavelength vs time, and (b) Relationship between wavelengths drift and air pressure.

experimental model with 104,587 elements. The parameters P and F are the water pressure and pulling force, respectively. The Young's modulus, Poisson's ratio, and density of the GFRP anchor rod were 41 GPa, 0.25, and 2000 kg/m^3, respectively.

Fig. 12 shows the strain measured by strain gauges installed on the surface of the GFRP anchor rod during the pulling process. It can be found that the simulated results were matched well with the measured results expect that the fluctuation measured by the transducer. The fluctuation may be induced by the particle rearrangement and strain dilation of soil mass during pullout process. The strains along the GFRP bar were increased during the pullout process which can be divided into three stages as indicated in Fig. 12. At stage A, the GFRP bar was in an elastic equilibrium state in which the strain was increased linearly with time. The GFRP bar was in a critical state or limit equilibrium state at stage B where the pullout out force was reached at the maximum static pullout force. At stage C, the interface between the GFRP bar and surrounding soil was reached in a plastic state where the GFRP bar was in the motion state. Although the simulation can not consider the irregular interface between the GFRP bar and the surrounding soil, the simulated results captured the phenomenon well.

Fig. 13 shows the simulated and measured earth pressure and pore water pressure during the pullout process. The simulated and experimental results matched well except that there are some deviation. The deviation can be attributed to the nonlinear behaviors of soil mass that are difficult to simulate by the numerical model, such as the soil dilation, particle rearrangement, and irregular interface between the GFRP bar and surrounding soil. However, the maximum deviation between the measured and simulated earth pressure was less than 6% which was less by considering the complex experimental boundary conditions and nonlinear plastic interface between the GFRP bar and surrounding soil. The numerical analysis indicates that the transducer has excellent performance in measuring both water and earth pressure in soil mass.

5. Conclusions

A new type of earth and water pressures transducer was proposed using the 3D FDM approach to measure the effective stress in soil mass. The transducer was designed with three layers to satisfy the needs of measuring earth pressure, water pressure and effective stress. The working principle and design details of the proposed hybrid pressure transducer were expounded. The calibration experiments and verification tests were conducted. Major conclusions are summarized as follows:

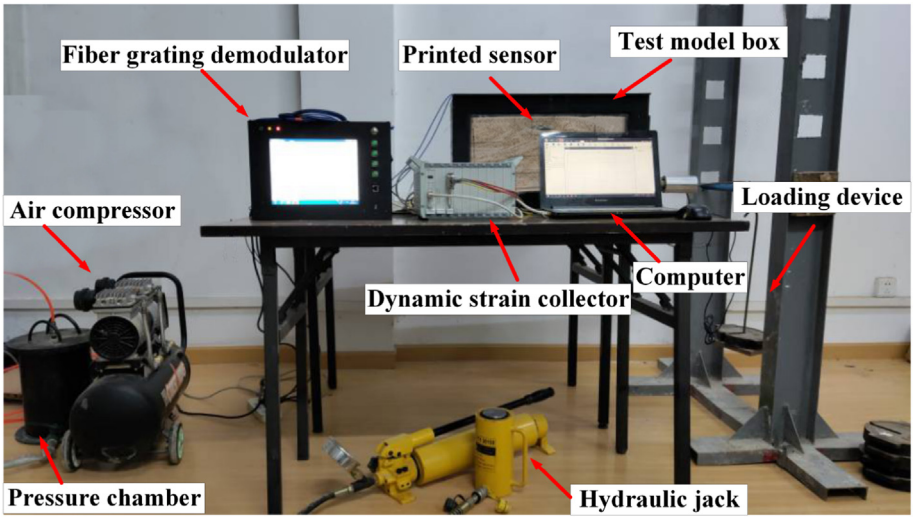

Fig. 9. Setup of the model test verification.

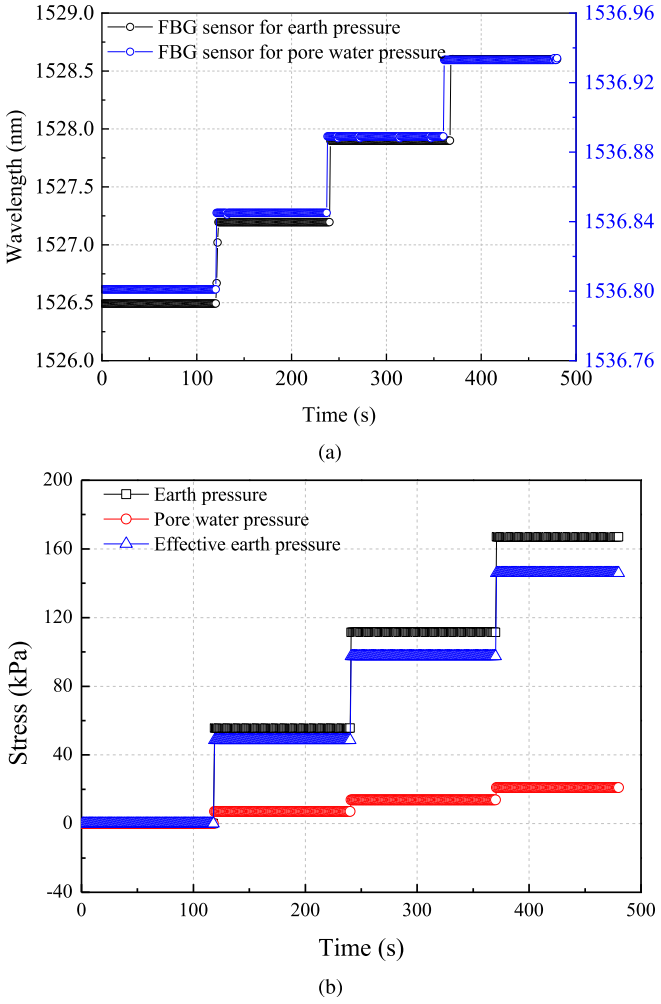

Fig. 10. Pullout test results: (a) Wavelength drift of FBG sensors in the transducer, and (b) Pressure measurements of the designed transducer.

(1) A hybrid transducer with integrated FBG sensors for earth and water pressure measurements in soil mass was designed and fabricated with the 3D FDM approach. Temperature compensation was taken into consideration by using a separate FBG temperature sensor. The encapsulation method was convenient for fabrication and of good deformation compatibility in soil mass.

(2) The calibration tests showed that the sensitivity coefficients for the measurement of earth and water pressures were 12.633 nm/MPa and 6.282 nm/MPa, respectively. Repeated tests and error analysis revealed that the designed transducer has high stability and sensitivity for earth pressure and water pressure measurement in soil mass.

(3) The performance of the transducer was further verified by a model experimental test together with numerical analysis.

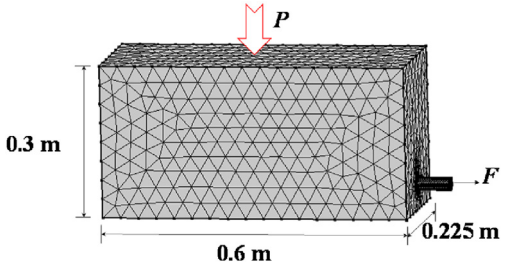

Fig. 11. Diagram of the simulation model.

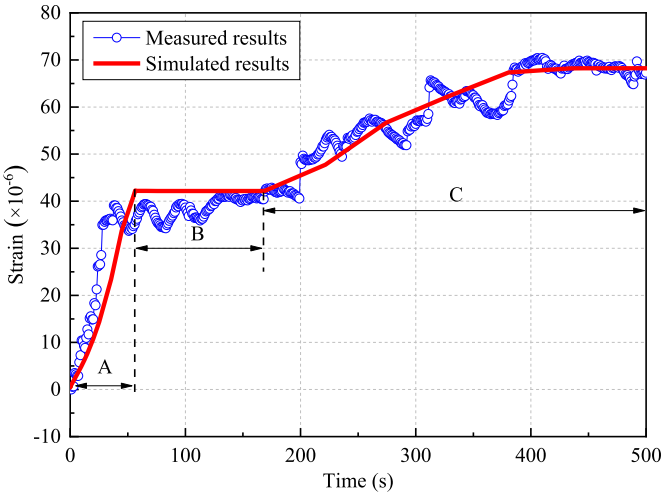

Fig. 12. Strain curves of anchor rod during pullout process.

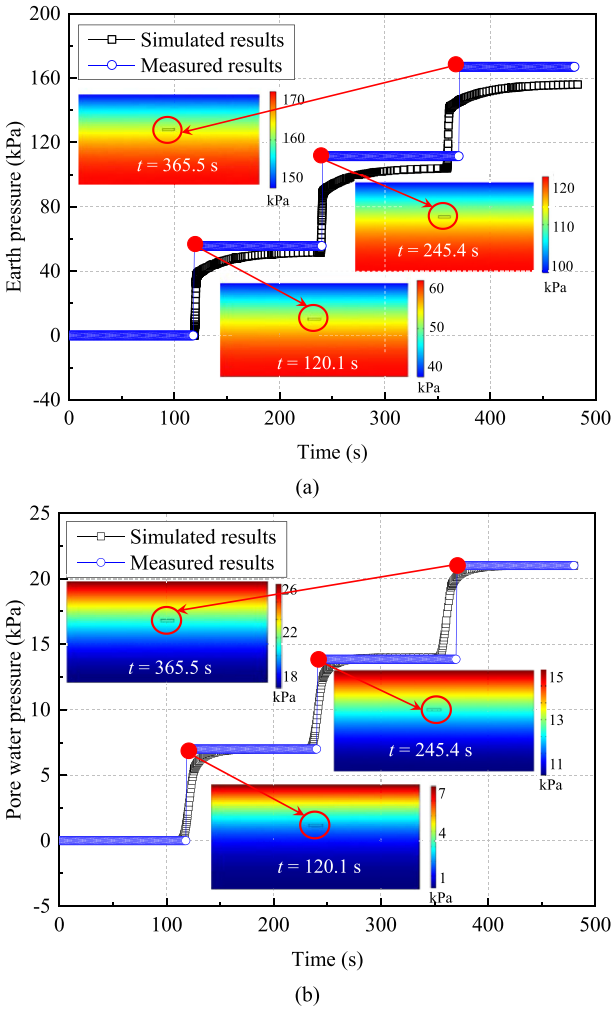

Fig. 13. Pressure–time curves: (a) Earth pressure, and (b) Pore water pressure.

The experimental and simulated tests matched well, finding a maximum measurement error of 6%. The transducer thus has promising practical applications with stable performance in engineering practices.

Declaration of competing interest

The authors declare that they have no known competing financial interests or personal relationships that could have appeared to influence the work reported in this paper.

Acknowledgments

We acknowledge the funding support from the National Natural Science Foundation of China (Grant Nos. 41972271 and 42177127) and Sanya Science and Education Innovation Park of Wuhan University of Technology (Grant No. 2020KF0007).

References

Cui, C.Y., Meng, K., Xu, C.S., Liang, Z.M., Li, H.J., Pei, H.F., 2021. Analytical solution for longitudinal vibration of a floating pile in saturated porous media based on a fictitious saturated soil pile model. Comput. Geotech. 131, 103942.
Garcia-Miquel, H., Barrera, D., Amat, R., Kurlyandskaya, G.V., Sales, S., 2016. Magnetic actuator based on giant magnetostrictive material Terfenol-D with strain and temperature monitoring using FBG optical sensor. Measurement 80, 201–206.
Gu, Y.F., Zhao, Y., Lv, R.Q., Yang, Y., 2016. A practical FBG sensor based on a thin-walled cylinder for hydraulic pressure measurement. IEEE Photon. Technol. Lett. 28 (22), 2569–2572.
Hill, K.O., Meltz, G., 1997. Fiber Bragg grating technology fundamentals and overview. J. Lightwave Technol. 15 (8), 1263–1276.
Hong, C.Y., Zhang, Y.F., Zhang, M.X., Leung, L.M.G., Liu, L.Q., 2016. Application of FBG sensors for geotechnical health monitoring, a review of sensor design implementation methods and packaging techniques. Sens. Actuators A Phys. 244, 184–197.
Hong, C.Y., Yuan, Y., Yang, Y.Y., Zhang, Y.F., Abro, Z.A., 2019a. A simple FBG pressure sensor fabricated using fused deposition modelling process. Sens. Actuators A Phys. 285, 269–274.
Hong, C.Y., Zhang, Y.F., Borana, L., 2019b. Design fabrication and testing of a 3D printed FBG pressure sensor. IEEE Access 7, 38577–38583.
Hong, C.Y., Zhang, Y.F., Yang, Y.Y., Yuan, Y., 2019c. A FBG based displacement transducer for small soil deformation measurement. Sens. Actuators A Phys. 286, 35–42.
Hu, Y.Q., Hong, C.Y., Zhang, Y.F., Li, G.W., 2018. A monitoring and warning system for expressway slopes using FBG sensing technology. Int. J. Distributed Sens. Netw. 14 (5), 1–12.
Li, H.J., Zhu, H.H., Li, Y.H., Hu, W., Shi, B., 2021. Fiber Bragg grating–based flume test to study the initiation of landslide-debris flows induced by concentrated runoff. Geotech. Test J. 44 (4), 20190290.
Li, T.L., Shi, C.Y., Ren, H.L., 2017. A novel fiber Bragg grating displacement sensor with a sub-micrometer resolution. IEEE Photon. Technol. Lett. 29 (14), 1199–1202.
Majumder, M., Gangopadhyay, T.K., Chakraborty, A.K., Dasgupta, K., Bhattacharya, D.K., 2008. Fiber Bragg gratings in structural health monitoring – present status and applications. Sens. Actuators A Phys. 147 (1), 150–164.
Meng, K., Cui, C.Y., Li, H.J., 2020. An ontology framework for pile integrity evaluation based on analytical methodology. IEEE Access 8, 72158–72168.
Pachava, V.R., Kamineni, S., Madhuvarasu, S.S., Putha, K., 2014. A high sensitive FBG pressure sensor using thin metal diaphragm. J. Opt. 43 (2), 117–121.
Pei, H.F., Jing, J.H., Zhang, S.Q., 2020. Experimental study on a new FBG-based and Terfenol-D inclinometer for slope displacement monitoring. Measurement 151, 107172.
Singh, A.K., Berggren, S., Zhu, Y., Han, M., Huang, H., 2017. Simultaneous strain and temperature measurement using a single fiber Bragg grating embedded in a composite laminate. Smart Mater. Struct. 26 (11), 115025.
Song, H.B., Pei, H.F., Xu, D.S., Cui, C.Y., 2020. Performance study of energy piles in different climatic conditions by using multi-sensor technologies. Measurement 162, 107875.
Tang, J.Y., Xu, D.S., Liu, H.B., 2018. Effect of gravel content on shear behavior of sand-gravel mixture. Rock Soil Mech. 39 (1), 93–102.
Wang, M., Li, X., Chen, L.H., Hou, S.Q., Wu, G.Y., Deng, Z.L., 2020. A modified soil water content measurement technique using actively heated fiber optic sensor. J. Rock Mech. Geotech. Eng. 12 (3), 608–619.
Wei, H.Z., Xu, D.S., Meng, Q.S., 2018. A newly designed fiber-optic based earth pressure transducer with adjustable measurement range. Sensors 18 (4), 932.
Wu, H., Zhu, H.H., Zhang, C.C., Zhou, G.Y., Zhu, B., Zhang, W., Azarafza, M., 2020. Strain integration-based soil shear displacement measurement using high-resolution strain sensing technology. Measurement 166, 108210.
Xu, D.S., 2017. A new measurement approach for small deformations of soil specimens using fiber Bragg grating sensors. Sensors 17 (5), 1016.
Xu, D.S., Dong, L.J., Borana, L., Liu, H.B., 2017. Early-warning system with quasi-distributed fiber optic sensor networks and cloud computing for soil slopes. IEEE Access 5, 25437–25444.
Xu, D.S., Liu, H.B., Luo, W.L., 2018. Development of a novel settlement monitoring system using fiber-optic liquid-level transducers with automatic temperature compensation. IEEE Trans. Instrum. Meas. 67 (9), 2214–2222.
Xu, D.S., Tang, J.Y., Zhou, Y., Rui, R., Liu, H.B., 2019. Macro and micro investigation of gravel content on simple shear behavior of sand-gravel mixture. Construct. Build. Mater. 221 (10), 730–744.
Xu, D.S., Xu, X.Y., Li, W., Fatahi, B., 2020a. Field experiments on laterally loaded piles for an offshore wind farm. Mar. Struct. 69, 102684.
Xu, D.S., Liu, Q.C., Qin, Y., Chen, B., 2020b. Analytical approach for crack identification of glass fiber reinforced polymer–sea sand concrete composite structures based on strain dissipations. Struct. Health Monit. 1475921.
Xu, D.S., Huang, M., Zhou, Y., 2020c. One-dimensional compression behavior of calcareous sand and marine clay mixtures. Int. J. GeoMech. 20 (9), 04020137.
Yang, Y.Y., Hong, C.Y., Abro, Z.A., Wang, L., Zhang, Y.F., 2019. A new fiber Bragg grating sensor based circumferential strain sensor fabricated using 3D printing method. Sens. Actuators A Phys. 295, 663–670.
Zhang, Y.F., Hong, C.Y., Ahmed, R., Ahmed, Z., 2017. A fiber Bragg grating based sensing platform fabricated by fused deposition modeling process for plantar pressure measurement. Measurement 112, 74–79.
Zhao, Y., Zheng, H.K., Lv, R.Q., Yang, Y., 2018. A practical FBG pressure sensor based on diaphragm-cantilever. Sens. Actuators A Phys. 279, 101–106.
Zhou, W.H., Tan, F., Yuen, K.V., 2018. Model updating and uncertainty analysis for creep behavior of soft soil. Comput. Geotech. 100, 135–143.
Zhou, W.H., Jing, X.Y., Yin, Z.Y., Geng, X.Y., 2019. Effects of particle sphericity and initial fabric on the shearing behavior of soil-rough structural interface. Acta Geotech 14 (66), 1699–1716.
Zhou, W.H., Qi, X.H., 2019. Root cohesion estimation of riparian trees based on model uncertainty characterization. J. Mater. Civ. Eng. 31 (2), 04018389.
Zhu, H.H., Ho, A.N.L., Yin, J.H., Sun, H.W., Pei, H.F., Hong, C.Y., 2012. An optical fiber monitoring system for evaluating the performance of a soil nailed slope. Smart Struct. Syst. 9 (5), 393–410.
Zhu, H.H., Shi, B., Yan, J.F., Zhang, J., Zhang, C.C., Wang, B.J., 2014. Fiber Bragg grating-based performance monitoring of a slope model subjected to seepage. Smart Struct. Syst. 23, 095027.
Zhu, H.H., Shi, B., Yan, J.F., Zhang, J., Wang, J., 2015. Investigation of the evolutionary process of a reinforced model slope using a fiber-optic monitoring network. Eng. Geol. 186, 34–43.
Zhu, H.H., Shi, B., Zhang, C.C., 2017. FBG-based monitoring of geohazards: current status and trends. Sensors 17 (3), 452.

Dongsheng Xu obtained his MSc degree from the Institute of Rock and Soil Mechanics, Chinese Academy of Sciences (CAS) and PhD degree from The Hong Kong Polytechnic University. He is professor of Geotechnical Engineering at the Wuhan University of Technology, and he is the head of the research center of Smart Infrastructure and Safety Protection (SISP), School of Civil Engineering and Architecture, Wuhan University of Technology. He has been involved in geotechnical and geology engineering research for more than 10 years. He is in charge of three projects supported by the National Natural Science Foundation of China including the National Science Fund for Excellent Young Scholars and eight research projects funded by Power China, China Railway Construction Corporation Limited, China Highway Engineering Consultants Corporation, and others. He has authored over 50 papers and 7 national patents. He is served as a council member of committee for Ocean Engineering Geology and Intelligent Monitoring Branch of Geology and Geotechnical Engineering.